


Reversal of effects from gel production in a reacting flow dependent on gel strength

Sae Hirano, Yuichiro Nagatsu , and Ryuta X. Suzuki *

*Department of Chemical Engineering, Tokyo University of Agriculture and Technology,
Naka-cho 2-24-16, Koganei, Tokyo 184-8588, Japan*



(Received 10 August 2021; accepted 26 January 2022; published 16 February 2022)

In reacting flows where chemical reactions occur within a flowing fluid, certain changes in the properties of the fluid, induced by the chemical reaction, can alter the flow dynamics. Generally, the most significant changes in the flow characteristics are associated with the largest changes in the fluid properties induced by the reaction. Specifically, the flow changes monotonically in response to the change in the physical properties induced by the reaction. However, this paper demonstrates a reacting liquid flow where the effect on the flow reverses in response to changes in the physical properties. We experimentally investigated viscous fingering (VF) in a reacting flow where the chemical reaction produces a gel. VF is a phenomenon wherein the interface of two fluids is fluid-dynamically unstable and forms a fingerlike pattern when the more-viscous fluid is displaced by the less-viscous one in porous media or Hele-Shaw cells. Rheological measurements of the gel produced at the liquid-liquid interface demonstrate that gel production affects the VF dynamics in completely opposing manners, depending on the strength of the gel. The VF pattern is approximately the same as the nonreactive case when the gel strength is weak, the fingers become narrower when the gel strength is medium, and the fingers become wider when the gel strength is strong. These opposing trends cannot be explained by standard linear stability analysis for a reactive system where only the viscosity effect is considered. In this paper, we propose a model that explains these opposite effects via a stability analysis of the VF that considers the strength and viscoelastic properties of the gel. In the proposed model, the VF becomes thinner when the shear thinning viscosity of the gel is effective, whereas the VF becomes wider when the gel behaves as an elastic or solid material and, thus, acts to reduce the permeability of the porous media. The aforementioned viscoelastic properties are based on actual viscosity measurements of the gel bulk itself. Combining the experimental results and theoretical considerations, we demonstrate that it is possible to achieve opposite VF effects depending on the gel strength. This is enabled by the fact that the rheological properties, which are primarily responsible for the flow dynamics, change depending on the gel strength.

DOI: [10.1103/PhysRevFluids.7.023201](https://doi.org/10.1103/PhysRevFluids.7.023201)

I. INTRODUCTION

Reacting flows in which chemical reactions occur within a flowing fluid, can be seen in a wide variety of fields, such as in industrial, environmental, and biological applications [1]. In reacting flows, the flow characteristics change when the physical properties of the fluid related to the flow (density, viscosity, interfacial tension, and viscoelasticity) change due to the reaction. Various experimental and theoretical studies on reacting flows have been performed, focusing on the chemical reaction-induced modification of flow dynamics via changes in density [2–20], viscosity

*Corresponding author: ryuta.x.suzuki@gmail.com

[21–36], interfacial tension [37–41], and viscoelasticity [42–49]. One such study reviewed previous studies on the effects of reaction-induced changes in density and viscosity on hydrodynamics [50]. Generally, the ratio between the reaction rate and flow rate, which is known as the Damköhler number (Da), significantly influences the reacting flow dynamics. Additionally, the variation in the physical properties induced by the reaction is also a significant factor. Given the same Da , or in an infinite Da condition with a very high reaction rate, typically, the influence of the reaction on the flow increases as the variation in the physical properties induced by the reaction increases. These effects, induced by density changes, viscosity changes, change in interfacial tension, and change in viscoelasticity, were reported in Refs. [2–6,8,10,12,13,16–18,20,21,23–25,29,31,34–36,41,46], respectively. Essentially, the flow changes monotonically in response to the changes in the physical properties induced by the reaction. However, in the present paper, we demonstrate, an observation of reversals in the flow dynamics induced by the reaction, dependent on the changes in the physical properties of the fluid. This finding was obtained in a reacting flow that produces a viscoelastic gel.

In the present paper, we investigated the viscous fingering (VF) phenomenon as a flow field. VF or Saffman-Taylor instability is a phenomenon where the interface of two fluids is hydrodynamically unstable. This induces a fingerlike configuration where the more viscous fluid is displaced by the less viscous liquid within a porous media or a Hele-Shaw cell—a thin gap between parallel plates, which is considered the simplest model of two-dimensional flow in porous media [51,52]. Generally, VF is classified according to the miscibility of the two fluids. When immiscible, the capillary number, which is the ratio of the interfacial tension and viscous force, is the dominant dimensionless number governing the behavior of the flow; and when miscible, the Péclet number, which is the ratio of the mass transport rate by convection and that by diffusion, is the dominant dimensionless number. The characteristics of VF with Newtonian fluids have been well investigated [52]. For both systems, the nonlinear propagation of VF is governed by multiple mechanisms including shielding and spreading and splitting. Shielding is the phenomenon in which a finger slightly ahead of its neighboring fingers quickly outruns them and shields them from further growth. Spreading and splitting are the phenomena in which a finger spreads until it reaches a certain width and becomes unstable and splits [52]. It is known that the non-Newtonian property of a fluid has great influence on the VF pattern. Experiments on materials, such as clay slurries, colloidal fluids, and polymer solutions, revealed branched fractal or fracturelike patterns [53–56]. The physical origin of the significantly different structures is so far unclear, mainly because these fluids simultaneously display multiple non-Newtonian properties, such as shear thinning or thickening, viscoelasticity, and yield stress. Therefore, numerous studies have been conducted on VF in non-Newtonian fluids with the aim of elucidating how each non-Newtonian property affects the VF formation. This was accomplished using fluids which can be regarded as having only one non-Newtonian property so that other non-Newtonian properties can be neglected [57–62]. In addition to the non-Newtonian fluid properties, chemical reactions occurring at the interface between the two fluids have attracted significant research attention because such reactions affect the VF dynamics. Both experimental and theoretical studies have reported changes in the VF pattern induced by changes in viscosity due to chemical reactions in the miscible systems [21–36]. In the immiscible system, changes were reported in the VF pattern induced by changes in the interfacial tension due to chemical reactions [37,39,41]. Additionally, a number of studies, including the present paper, have been conducted on VF in the presence of gel production. For miscible systems, Nagatsu *et al.* [46] reported that the VF pattern changes to a spiral pattern due to gel formation. For immiscible systems, a report by Niroobakhsh *et al.* [48] demonstrated that a wide variety of fingering patterns can be observed depending on the reactant concentration and flow rate, which are strikingly different from classic VF instability.

Not limited to VF, several studies have also been conducted on reacting flows that produce gels or viscoelastic materials [43–45,47,49]. Significant attention has been paid to the elastic fingering phenomenon, which is induced in gel-like materials due to a chemical reaction during fluid displacement in the Hele-Shaw cell [42,63–67] (elastic fingering can be distinguished from VF because it is induced mainly by the elastic properties). However, no studies have systematically

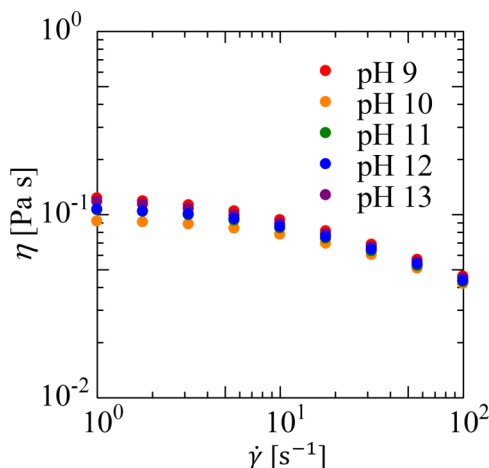
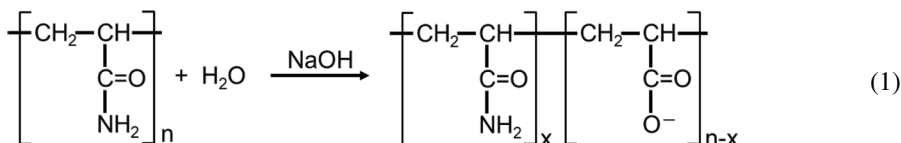


FIG. 1. Shear viscosity for the polymer solutions with varying pH .

changed the viscoelastic strength of the gels produced and clarified the effects in detail. In this paper, we combine a reacting flow experiment, which produces gel via VF and the rheological measurements of the gel. We demonstrate that the VF pattern is the same as in a nonreactive flow when the gel strength is weak, becomes narrower when the gel strength is medium, and becomes wider when the gel strength is high. These results indicate that the flow dynamics reverse depending on the degree of change in the physical properties of the fluid induced by the gel production reaction in the reacting flow, which has, thus, far not been clearly demonstrated. We demonstrate that these opposite effects cannot be explained using a standard linear stability analysis for reactive miscible VF [36] where only the influence of the viscosity is considered. Alternatively, we propose a simple model for the stability of VF that considers the viscoelastic effects of the gel produced, which can explain the opposite effects.

II. SOLUTION SYSTEM AND MEASUREMENT OF FLUID PROPERTIES

In this paper, we employed a 1.00-wt% partially hydrolyzed polyacrylamide (HPAM) solution as the more viscous fluid and a 0.1-M $\text{Fe}(\text{NO}_3)_3$ solution as the less viscous fluid. To alter the strength of the gels produced whereas maintaining the viscosities of the polymer solutions, we changed the pH of the polymer solution by diluting the polymer solution with an aqueous solution of NaOH, instead of water. When the aqueous solution of NaOH was added to the PAM solution, a portion of the amide groups in the PAM was hydrolyzed to form carboxylate groups [Eq. (1)] [68]. Both the PAM (weight-average molecular weight: $M_w = 5 \times 10^6$) and the NaOH were obtained from WAKO Pure Chemical Industries, Ltd. without further purification. We prepared polymer solutions with pH values ranging from 9 to 13. Prior to the VF experiment, we measured the shear viscosity using an AR-G2 rheometer from TA Instruments. The results of these measurements are presented in Fig. 1. The polymer solutions have approximately the same viscosity but have a shear-thinning property. The density was measured by a pycnometer: the densities of the polymer solutions of pH 9, 10, 11, 12, 13, and that of the 0.1-M $\text{Fe}(\text{NO}_3)_3$ solution were 1.001, 1.001, 1.001, 1.001, 1.003, and 1.126 g/cm^3 , respectively. However, the effect of the density can be negligible in a horizontal Hele-Shaw flow when the gap is sufficiently small as in this paper,



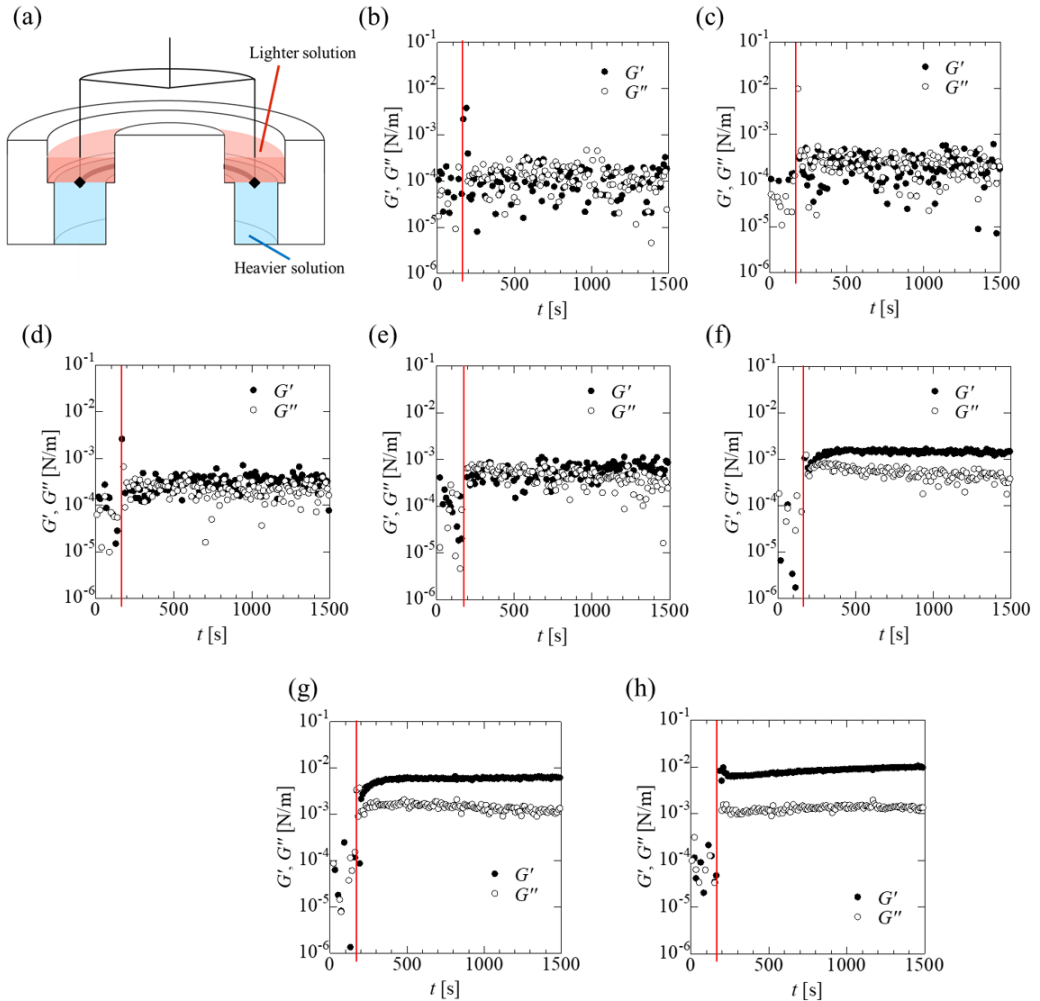


FIG. 2. (a) Schematics of the double wall ring geometry for an interfacial shear rheometry. Time-sweep measurement of the liquid-liquid interfacial rheology between (b) pH 9, (c) pH 10, (d) pH 11, (e) pH 11.5, (f) pH 12, (g) pH 12.5, and (h) pH 13 of polymer solution and $Fe(NO_3)_3$ solution with 1% strain and frequency of 0.2 Hz. At $t = 180$ s, which is drawn by red solid lines, the $Fe(NO_3)_3$ solution contacts the polymer solutions.

(ii) G' and G'' having a cross-over point with ω , demonstrates a concentrated solution of a polymer.

(iii) G' and G'' being constant as ω is changed whereas η^* decreases as ω demonstrates gel.

The results for solutions with pH of 9 or 10 indicate a dilute solution, i.e., no or little gel is produced because both G' and G'' are relatively small, and approximately $\tan \delta = 1$. Also, the result for pH 11 or 11.5 indicates that the solution has weak gel property because both G' and G'' are relatively larger, and $\tan \delta$ is smaller than 1. However, the measurements for solutions with pH of 12, 12.5, or 13 demonstrate that gel is produced since both G' and G'' are almost constant against ω [Figs. 4(e)–4(g)], and the gel produced is stronger as pH is larger because G' and G'' are greater and $\tan \delta$ is smaller as pH is larger. The results presented in Figs. 2–4 demonstrate that gel is effectively not produced when the pH are 9 and 10, the gel produced at a pH of 11 is weak, medium at a pH of 12, and strong at a pH of 13.

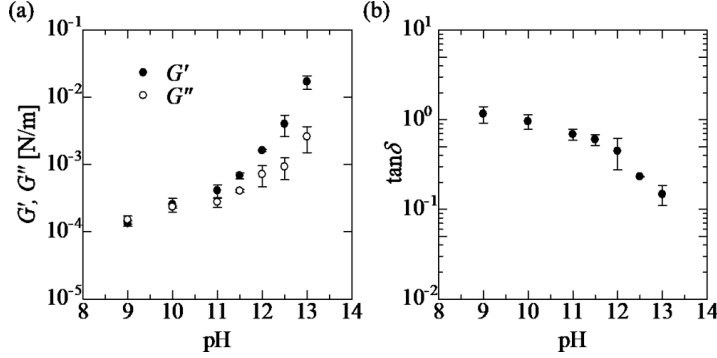


FIG. 3. (a) Measured storage and loss moduli and (b) $\tan \delta$ calculated based on (a) for several pH . The error bars indicate standard deviation.

III. VF EXPERIMENT

The VF experiments in this paper were conducted using a radial Hele-Shaw cell, which consists of two parallel glass plates ($140 \times 140 \text{ mm}^2$) with a 0.5-mm gap between the plates. First, the flow through a porous media is expressed by Darcy's law,

$$\vec{u} = -\frac{k}{\eta} \nabla p, \quad (3)$$

where \vec{u} is the velocity of the flow through the porous media, k is the permeability of the porous media, η is the viscosity of the fluid, and p is the pressure. The flow in Hele-Shaw cells is expressed as

$$\vec{u} = -\frac{b^2}{12\eta} \nabla p, \quad (4)$$

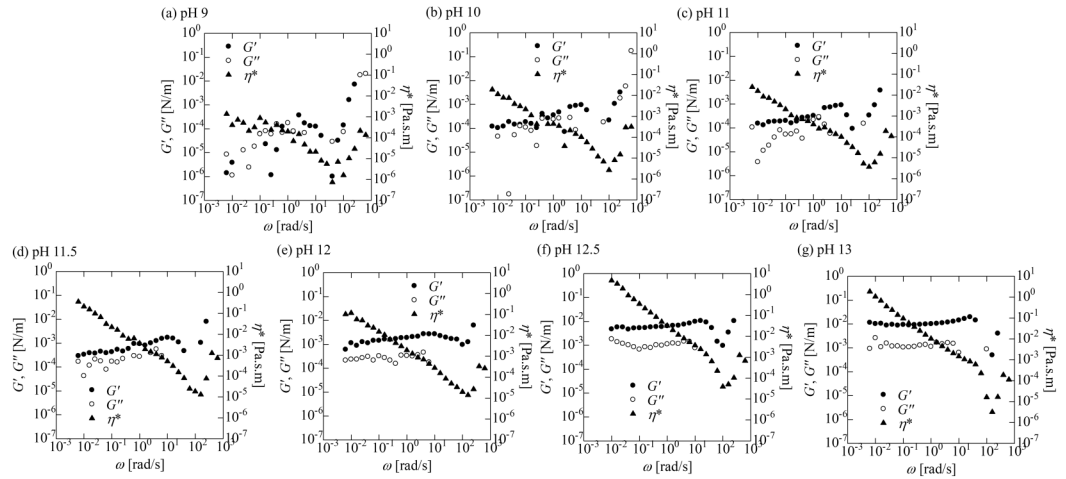


FIG. 4. Frequency sweep measurement of the liquid-liquid interfacial rheology between (a) pH 9, (b) pH 10, (c) pH 11, (d) pH 11.5, (e) pH 12, (f) pH 12.5, and (g) pH 13 of polymer solution and $\text{Fe}(\text{NO}_3)_3$ solution with 1% strain.

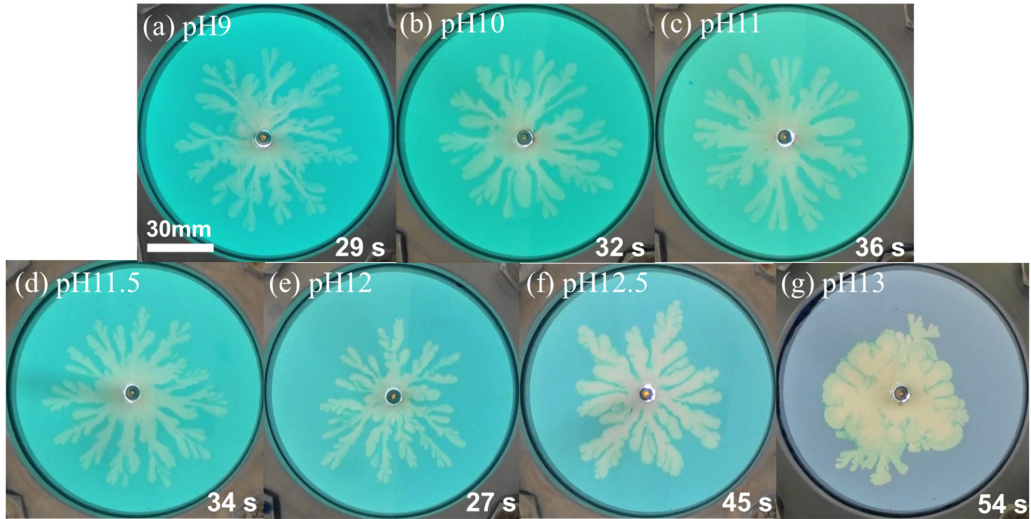


FIG. 5. Displacement results for (a) pH 9, (b) pH 10, (c) pH 11, (d) pH 11.5, (e) pH 12, (f) pH 12.5, and (g) pH 13 HPAM cases. The time shown at right bottom corner represents the time when the picture was taken (when the longest radius reaches 45 mm).

where b is the gap between the two parallel plates. Equations (1) and (2) are equivalent when $k = b^2/12$. Therefore, it is possible to visualize the flow through the porous media as the flow in Hele-Shaw cells. The flow rate employed in the present paper was 100 ml/h. The more viscous polymer solutions were dyed blue using 0.01-wt% methylene blue to visualize the displacement process. The displacement experiments were conducted a minimum of three times under each condition.

The observations made during the displacement of the HPAM solutions by the $Fe(NO_3)_3$ solution suggest that the strong gel stabilizes the finger pattern as shown in Fig. 5(g). The standard fingering patterns are observable at pH values ranging from 9 to 12.5 [Fig. 5(a)–5(f)]. However, upon a more detailed investigation, the fingers at a pH of 12, shown in Fig. 5(e), are narrower compared to the other fingers. At a pH of 12.5, somewhat wider finger are observed. Figure 6 presents the time evolution of fingers at a pH of 13. In these images, the cross-linking chemical reaction results in the production of gel at the interface between the displacing and the displaced solutions. This gel stabilizes the fingering pattern, making a circular pattern. However, the classical fingers appear at $t = 60$ s because the ferric ion Fe^{3+} has been consumed, and so the chemical reaction does not occur. Essentially, the concentration of the $Fe(NO_3)_3$ solution at the interface decreases with time. Therefore, to maintain the strength of the gel at the interface at all times, the concentration

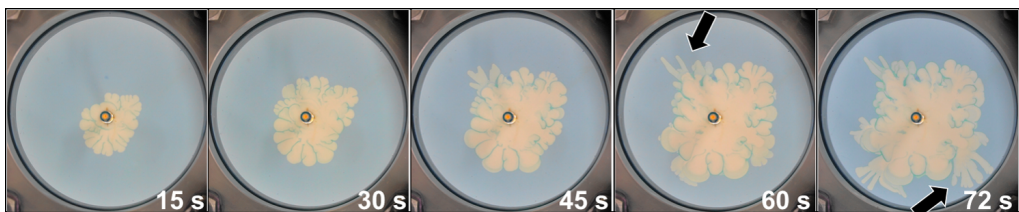


FIG. 6. Time evolution of the finger growth at pH 13. The black arrows show the classical fingering patterns because the chemical reaction of the cross-linking does not occur.

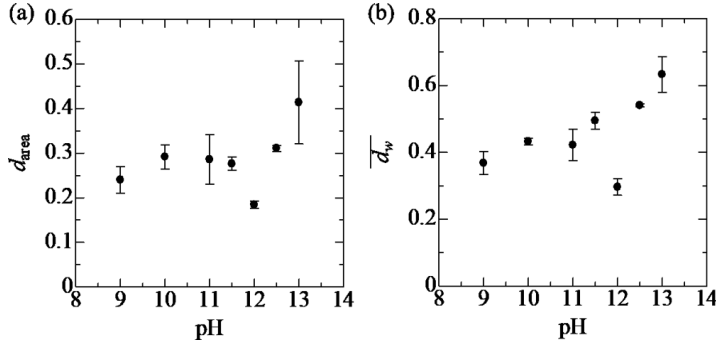


FIG. 7. Quantitative analyses for (a) the area density and (b) the finger width density.

of $\text{Fe}(\text{NO}_3)_3$ should be sufficiently large. In the present paper, the 0.1-M $\text{Fe}(\text{NO}_3)_3$ solution was sufficiently concentrated to maintain the cross-linking reaction when the volume ratio was 1, meaning 100 ml of HPAM was able to fully react with 100 ml of the 0.1-M $\text{Fe}(\text{NO}_3)_3$ solution. However, focusing on the interface, the concentration of the 0.1-M $\text{Fe}(\text{NO}_3)_3$ solution may be insufficient.

To analyze the pattern quantitatively, we utilized the area density d_{area} , (which is sometimes called the finger density) defined as the ratio of the area occupied by the pattern within the circle of radius r_{max} to the area of the circle πr_{max}^2 , where r_{max} is the longest radius [Fig. 7(a)] [21]. As expected, the d_{area} of pH 13 is the largest, and the d_{area} of pH 12 is the smallest. Focusing on the finger width, Fig. 7(b) shows the finger width density $\overline{d_w}$ [39], where d_w is a function of the radius r and is defined as the ratio of the average finger width \bar{w} to $2\pi r$. \bar{w} is measured using the intersection of concentric circles, centered on the injection point as a function of the circle radius r [48,72]. $\overline{d_w}$ is determined by averaging d_w over $r = 5\text{--}45$ mm. The results of the calculation of $\overline{d_w}$ are presented in Fig. 7(b), where $\overline{d_w}$ at a pH of 13 is much higher than that at a pH of 9–12 because of the VF stabilized by the gel produced in the reaction. Additionally, $\overline{d_w}$ has a nonmonotonic relation to the pH as the value of $\overline{d_w}$ is lowest at a pH of 12.

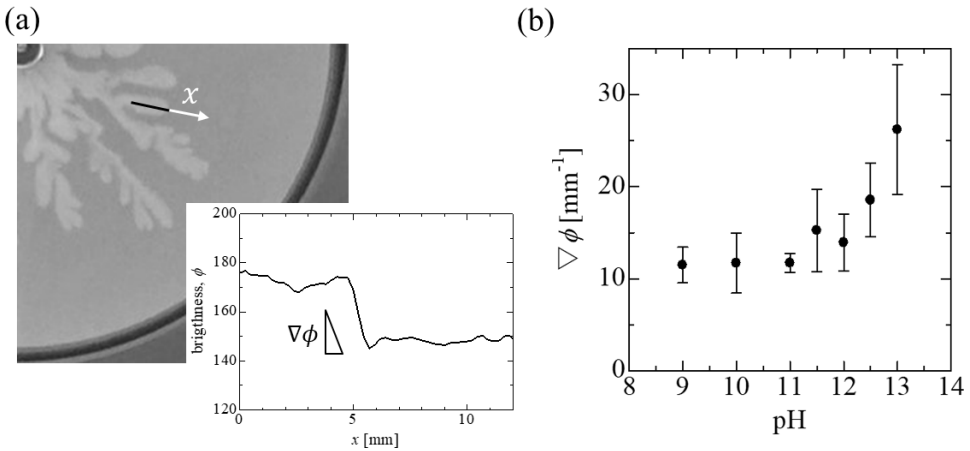


FIG. 8. Measurement of concentration profile in different pH fingering regimes. (a) The definition of $\nabla\phi$, which is the gradient of brightness and (b) the relation between $\nabla\phi$ and different pH fingering.

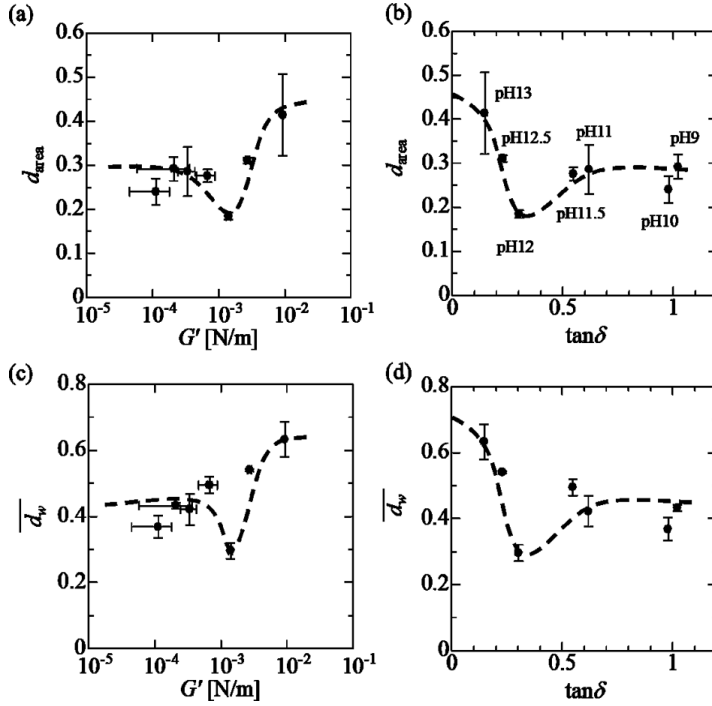


FIG. 9. (a) G' vs area density, (b) $\tan \delta$ vs area density, (c) G' vs width density, and (d) $\tan \delta$ vs width density.

Subsequently, the concentration gradient around the interface was investigated. Figure 8(a) presents a gradient of the brightness around the interface ϕ , which is defined as the amount of the gap that is filled by $\text{Fe}(\text{NO}_3)_3$ solution. It is calculated using the image processing program IMAGEJ as brightness divided by x , the interfacial length. Therefore, $\nabla\phi$ represents degree of miscibility over the gel interface. The value of $\nabla\phi$ was calculated from 15 measurement points at each $p\text{H}$ level. When the chemical reaction [Eq. (2)] was insufficient or the gel strength was too weak, the interface became miscible, and the finger pattern was similar to a classical miscible VF pattern as presented in numerous studies [52,73,74]. By contrast, when the chemical reaction produces a strong gel-like material at the interface, the interface becomes immiscible because the two solutions cannot mix with each other. A low value for $\nabla\phi$ means the interface is miscible, and a high value means that a gel is produced at the interface. From Fig. 8(b), we can confirm that the relation of $\nabla\phi$ to the $p\text{H}$ of the polymer solutions demonstrates monotonic behavior in which $\nabla\phi$ is effectively constant for $p\text{H}$ in the range of 9–11 and monotonically increases with $p\text{H}$ when $p\text{H}$ is larger than 11. These results demonstrate that either very little gel is produced, or the strength of the gel during VF formation is weak for solutions with $p\text{H}$ of 9–11, the strength is medium at a $p\text{H}$ of 12, and strong at a $p\text{H}$ of 13, which is consistent with the results of the interfacial rheological measurements described earlier.

The next step was to investigate the relation between the gel production effects on the VF pattern and the rheological properties of the gel. For this purpose, we plotted d_{area} vs G' , d_{area} vs $\tan \delta$, \overline{d}_w vs G' , and \overline{d}_w vs $\tan \delta$ in Figs. 9(a)–9(d), respectively. From these figures, it is clear that all of the relations demonstrated nonmonotonic behavior. These results clearly demonstrate that the gel has opposite effects on the VF dynamics depending on the gel strength. Specifically, the gel produced at a $p\text{H}$ of 12 decreases the d_{area} and \overline{d}_w compared to the cases with no gel or weak gel at $p\text{H}$ of 9–11; in contrast, the gel produced at $p\text{H}$ of 13 increases d_{area} and \overline{d}_w compared to the cases with no or weak gel at $p\text{H}$ of 9–11.

Here, we comment quantitative values to define what is weak, medium, or strong for the strength of the gel. In general, it is possible to quantitatively evaluate the gel strength by the absolute value of G' , G'' , and $\tan \delta$ and by the dependence of them on the frequency. Our main findings in the present paper are the effect of the gel production on VF dynamics are opposite, depending on the gel strength. Specifically, the VF pattern is approximately the same as the nonreactive case when the gel strength is weak, the fingers become narrower when the strength is medium, and the fingers become wider when the strength is strong. A threshold for the opposite effect are determined not only by the gel strength, but also by the viscosity of the more-viscous liquid and the flow rate. However, we find that we can classify the gel strength under the present condition of them as follows; $G' \sim 10^{-4}$ N/m, $\tan \delta \sim 1$ for no gel, $G' \sim 10^{-4} - 10^{-3}$ N/m, $\tan \delta \sim 0.6-0.7$ for weak gel, $G' \sim 10^{-3}$ N/m, $\tan \delta \sim 0.5$ for medium gel, and $G' > 10^{-3}$ N/m, $\tan \delta < 0.5$ for strong gel.

In the next section, we attempt to theoretically explain the opposite or nonmonotonic effects of the gel strength on the VF dynamics.

IV. THEORETICAL INVESTIGATION

A. Linear stability analysis

To conduct a stability analysis, we utilized the nondimensional governing equations provided by Hejazi *et al.* [36] as follows:

$$\nabla \cdot \vec{u} = 0, \quad (5)$$

$$\nabla p = -\eta(\vec{u} + \vec{i}), \quad (6)$$

$$\frac{\partial a}{\partial t} + \vec{u} \cdot \nabla a = \nabla^2 a - D_a a b, \quad (7)$$

$$\frac{\partial b}{\partial t} + \vec{u} \cdot \nabla b = \nabla^2 b - D_a a b, \quad (8)$$

$$\frac{\partial c}{\partial t} + \vec{u} \cdot \nabla c = \nabla^2 c + D_a a b, \quad (9)$$

$$\eta = \exp \{R_B b + R_C c\}, \quad (10)$$

$$R_B = \ln \left(\frac{\eta_B}{\eta_A} \right), \quad (11)$$

$$R_C = \ln \left(\frac{\eta_C}{\eta_A} \right), \quad (12)$$

where \vec{u} is the velocity vector; \vec{i} is the unit vector along x ; p is the pressure; η is the viscosity; a – c are the concentrations of the polymer $\text{Fe}(\text{NO}_3)_3$, and produced gel-like material, respectively. Note that these are all nondimensional variables. Da is the Damköhler number; and R is the logarithmic-viscosity ratio. It should be noted that this is a model for a Newtonian fluid. Subsequently, the standard linear stability analysis was conducted using Eqs. (5)–(12) following Hejazi *et al.* [36]. For the finite Da , the relation between growth rate σ and wave-number k is derived by Hejazi *et al.* [36] as follows:

$$\begin{aligned} & (e^{R_B} + 1)(\sqrt{k^2 + \sigma + D_a} + k)\{R_B k - 2\sqrt{k^2 + \sigma}(k + \sqrt{k^2 + \sigma})\} \\ & + k(e^{R_B} - 1)(R_C - R_B)(\sqrt{k^2 + \sigma} - \sqrt{k^2 + \sigma + D_a}) = 0. \end{aligned} \quad (13)$$

The dispersion results with different D_a s are presented in Fig. 10. To obtain the values of R_B and R_C , we directly measured η_A , η_B , and η_C using the rheometer and found $R_B = 4.83$, $R_C = 4.83$ at a pH of 9; $R_B = 4.83$, $R_C = 8.36$ at a pH of 12; and $R_B = 4.83$, $R_C = 10.2$ at a pH of 13. A detailed explanation of the viscosity measurement is included in the subsequent section. From Fig. 10, it

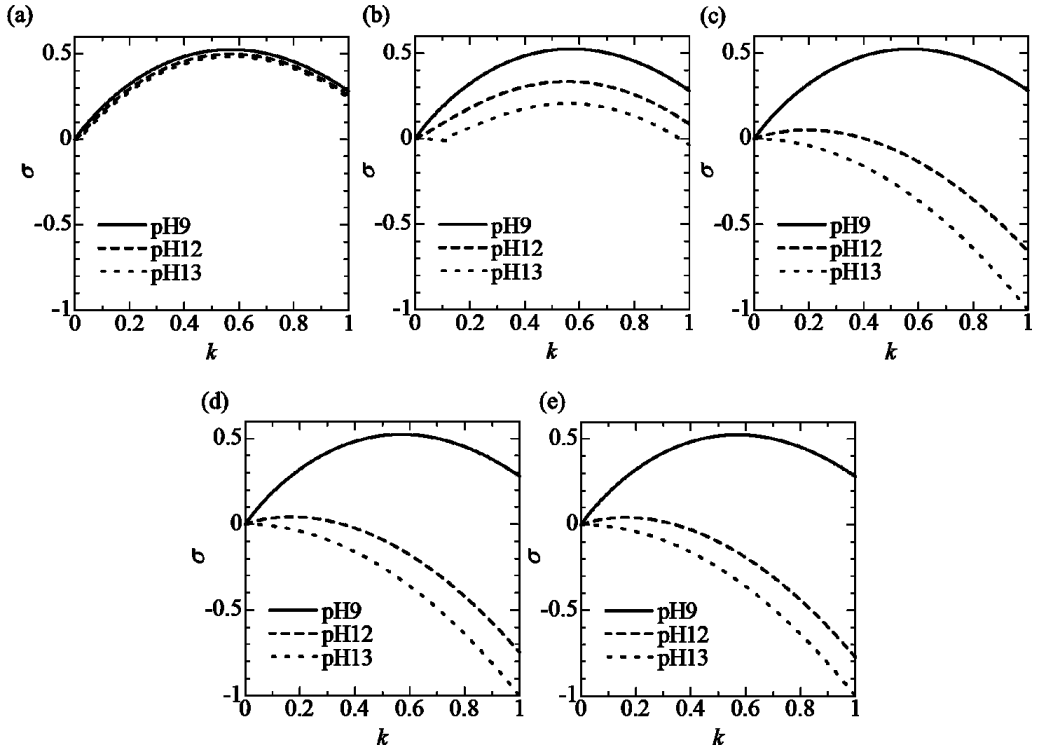


FIG. 10. Dispersion curves at $t_0 = 0$ showing the interface of Da for (a) $Da = 0.1$, (b) $Da = 1$, (c) $Da = 100$, (d) $Da = 10^3$, and (e) $Da = 10^4$.

is clear that the growth rate monotonically changes with the pH , even when the various reaction rates are considered. Therefore, this linear stability analysis alone cannot explain the nonmonotonic behavior, such as the area density and finger width density. Thus, a new model is required to explain this phenomenon, the details of which are described in the following subsection.

B. Proposed model

In this section, the mechanism by which the produced gel influences the VF dynamics is considered. We assumed that:

- (i) The chemical reaction is instantaneous.
- (ii) The situation is illustrated by Fig. 11, where u is velocity, z is the position, η is the viscosity, p is the pressure, L is the length of the porous media, and indices A and B represent the zone. δz is virtual displacement.

The flow in Hele-Shaw cells is expressed by Eq. (3) as presented in the Introduction. The flow in one dimension is expressed as

$$u = \frac{k}{\eta} \left(-\frac{dp}{dz} \right). \quad (14)$$

We consider that the less-viscous $\text{Fe}(\text{NO}_3)_3$ solution with viscosity η_1 flows left to right, displacing the more-viscous HPAM solution with η_3 , and the gel with viscosity η_2 is produced between the two solutions as is shown in Fig. 11. We assume the viscosity of the gel at zone B where the virtual displacement is imposed is slightly different than that at zone A and, thus, it is denoted as $\beta\eta_2$.

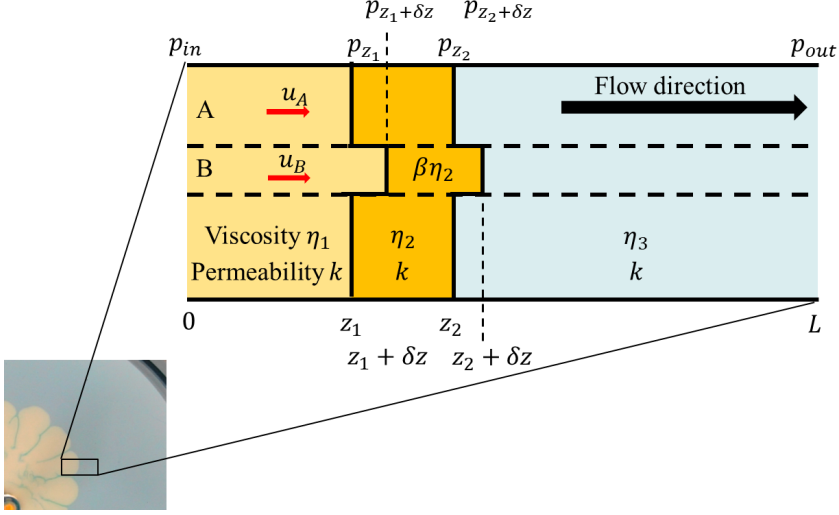


FIG. 11. Schematic of the Hele-Shaw flow near the interface between more- and less-viscous liquids (inset) for the present paper. The less viscous $\text{Fe}(\text{NO}_3)_3$ solution with viscosity η_1 flows left to right, displacing the more viscous HPAM solution with η_3 , and the gel with viscosity η_2 is produced between the two solutions in the figure. k is the permeability. We assume that the viscosity of the gel at zone B is slightly different than that at zone A, and, thus, it is denoted as $\beta\eta_2$.

Under this assumption, we obtain the following equation based on Eq. (14):

$$u_A - u_B = \frac{\eta_1 + (\beta - 1)\eta_2 \frac{z_2 - z_1}{\delta z} - \eta_3}{\eta_1 z_1 + \eta_2(z_2 - z_1) + u_A \eta_3(L - z_2)} u_B \delta z. \quad (15)$$

The derivation of Eq. (15) is described in the Supplemental Material [75]. Denoting $\frac{z_2 - z_1}{\delta z}$ as z' , Eq. (15) becomes

$$u_A - u_B = \frac{\eta_1 + (\beta - 1)z'\eta_2 - \eta_3}{\eta_1 z_1 + \eta_2(z_2 - z_1) + u_A \eta_3(L - z_2)} u_B \delta z. \quad (16)$$

Here, the denominator on the right side of Eq. (16) is positive because $\eta_1 - \eta_3$, $(z_2 - z_1)$, and $(L - z_2)$ are positive. When $u_A - u_B$ is positive, the virtual displacement becomes sufficiently small such that the interface finally becomes flat, which means no fingering occurs or that the system becomes hydrodynamically stable. In the opposite situation, when $u_A - u_B < 0$, the virtual displacement becomes enhanced, resulting in a VF pattern. Additionally, the case where $u_A - u_B < 0$ should be divided into two, namely, $(u_A - u_B)_{\text{reactive}} < (u_A - u_B)_{\text{nonreactive}} < 0$ and $(u_A - u_B)_{\text{nonreactive}} < (u_A - u_B)_{\text{reactive}} < 0$. In the former case, the VF dynamics become increasingly unstable due to the reaction. In the latter case, the VF dynamics become less unstable due to the reaction but are still hydrodynamically unstable. To evaluate $u_A - u_B$, the numerator in the right-hand side of Eq. (16) should be investigated. In this paper, the viscosity of the $\text{Fe}(\text{NO}_3)_3$ solution η_1 was 9.65×10^{-4} Pa s, the viscosity of the HPAM solution η_3 was 0.120 Pa s at $\dot{\gamma} = 1.4 \text{ s}^{-1}$, which were calculated from the injection rate of 100 ml/h at $r = 25$ mm using the equation, $U = \frac{q}{2\pi r b}$, and $\dot{\gamma}_f = \frac{q}{\pi R b^2}$, where U is the increase rate of the circle's radius R when the less-viscous liquid completely displaces the more-viscous liquid, keeping the boundary circular, and $\dot{\gamma}_f$ is the shear rate in the vicinity of the fingertip [21]. In addition, we roughly estimate the width of gel as $z_2 - z_1 \sim 1$ mm, and the virtual displacement as $\delta z \sim 0.1$ mm, and, thus, $z' \sim 10$. The phase diagram spanned by η_2 and $(\beta - 1)$ for effect of the gel production on the VF dynamics is presented in Fig. 12, which was obtained using the aforementioned values of η_1 , η_3 , and z' . The physical meaning of the horizontal axis $(\beta - 1)$

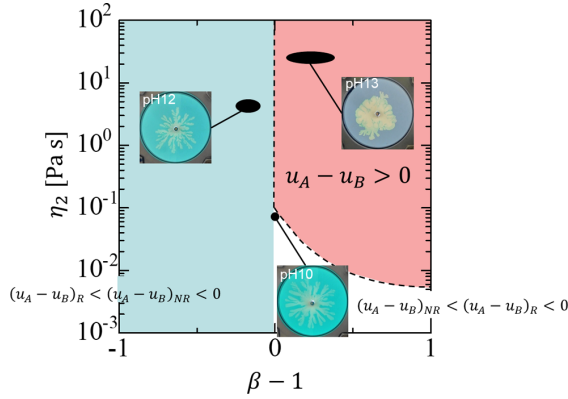


FIG. 12. Phase diagram spanned by $(\beta - 1)$ and η_2 for the effect of the gel production on the VF dynamics. When the condition is in the stable region, the pattern is stable and is circular. The standard fingering patterns are observable at the unstable region. At the more unstable region, the fingers are narrower than those without the produced gel. $(u_A - u_B)_R$ and $(u_A - u_B)_{NR}$ represent $(u_A - u_B)_{\text{reactive}}$ and $(u_A - u_B)_{\text{nonreactive}}$, respectively.

is whether the gel viscosity effectively increases or decreases by the virtual displacement. In the diagram, the stable and unstable zones, determined based on whether $u_A - u_B$ is positive or negative, are shown. The dashed line represents $u_A - u_B = 0$, and the red region represents $u_A - u_B > 0$. The blue region demonstrates that $u_A - u_B$ of the reactive system is more negative than $u_A - u_B$ of the nonreactive VFs without produced gel, namely, $(u_A - u_B)_{\text{reactive}} < (u_A - u_B)_{\text{nonreactive}} < 0$. When $(\beta - 1)$ becomes negative, $u_A - u_B$ is more negative than $u_A - u_B$ without the reaction at all times, and the VF dynamics become more unstable due to the reaction. When the viscosity of the gel is large and $(\beta - 1)$ is positive and large, $u_A - u_B$ is positive, and the virtual displacement is suppressed.

It is important to know the viscosity of the gel to identify the cases for pH 12 and 13 in the diagram. Therefore, we measured the viscosity of the gel bulk itself, which is obtained by mixing the two solutions [HPAM at a pH of 12 and 13 and the 0.1 M $\text{Fe}(\text{NO}_3)_3$] in equal volumes in a beaker, using a rheometer and a cone plate. The results are presented in Fig. 13. Figure 13 shows that:

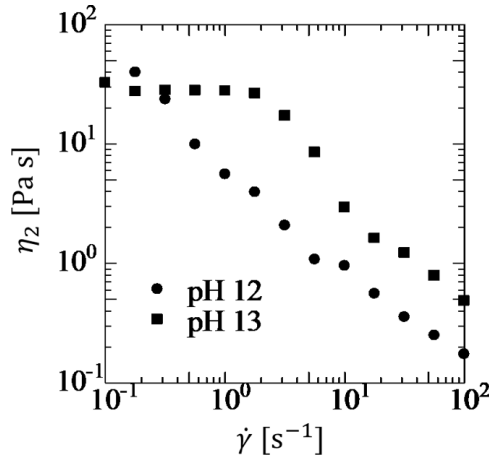


FIG. 13. Results of shear viscosity measurement of the gel using cone plates.

- (i) The gel produced at a pH of 12 demonstrates shear-thinning viscosity behavior.
- (ii) The gel produced at a pH of 13 demonstrates shear-thinning viscosity over approximately $\dot{\gamma} = 2 \text{ s}^{-1}$, whereas it has constant viscosity when less than $\dot{\gamma} = 2 \text{ s}^{-1}$.

Therefore, the difference between the gels produced at pH values of 12 and 13 is whether the gel demonstrates shear-thinning viscosity behavior. At a pH of 12, the shear-thinning viscosity behavior indicates that the value of $(\beta - 1)$ should be negative. This is because the shear rate imposed on zone B is larger than that imposed on zone A . This consideration leads to $\beta < 1$ for the fluids having shear thinning viscosity. Therefore, the case with pH 12 can be located in the blue region. Specifically, an estimated zone where the case with pH 12 is located in a black ellipse in the blue zone since $\eta_{2, pH=12} = 4.11 \text{ Pa s}$, which is the value at $\dot{\gamma} = 1.4 \text{ s}^{-1}$ (Fig. 13). On the other hand, for pH 13, we consider that the constant viscosity of the gel against the shear rate and that the gel behaves as a solid, which acts to reduce the permeability. The reduction of permeability means a decrease in mobility k/η . The influence of this decrease is similar to the effect that would be obtained by an increase in viscosity, which leads to a positive $(\beta - 1)$. Additionally, the viscosity of the gel at a pH of 13 is $\eta_{2, pH=13} = 27.1 \text{ Pa s}$, which is the value at $\dot{\gamma} = 1.4 \text{ s}^{-1}$ (Fig. 13). Therefore, the case with pH 13 can be located in a black ellipse in the red region because $\eta_2 = 27.1 \text{ Pa s}$ and $0 \leq (\beta - 1)$ is possible. Note that the location of the case with pH 10 is indicated by a black circle because the gel is hardly produced, resulting in $\eta_{2, pH=10}$ being equal to η_3 (which is 0.120 Pa s at $\dot{\gamma} = 1.4 \text{ s}^{-1}$) and $\beta = 1$. To summarize, using the proposed model, when the shear thinning viscosity property of the gel is produced at a pH of 12 and the elastic property of the gel is produced with sufficiently high viscosity at a pH of 13 acting to reduce the permeability, which are based on actual measurements (Fig. 13), we can explain the opposite effects of the gel production on the VF dynamics. Therefore, the proposed model demonstrates that the opposite effects, depending on the gel's strength, is driven by the fact that the rheological properties, which are mainly responsible for the flow dynamics, change depending on the gel strength.

V. CONCLUSIONS

In this paper, the effects of gel production at the liquid-liquid interface on VF dynamics were investigated using the displacement of the more viscous HPAM solutions with variable pH by a less-viscous $\text{Fe}(\text{NO}_3)_3$ solution in a radial Hele-Shaw cell along with the corresponding rheological measurements. We found that the VF pattern is the same as for the nonreactive one when the gel strength is weak becomes narrower when the gel strength is medium and becomes wider when the gel strength is high. These results demonstrate that the gel production can have opposite effects on VF dynamics depending on the gel strength. A linear stability analysis of the reactive system developed by Hejazi *et al.* [36], which is a model for a Newtonian fluid where only the viscosity effect is considered, was not able to explain the opposing effects. We were able to develop a simple model of the stability of VF, which can explain the opposite effects by considering the viscoelastic effects of the gel produced in the reaction. In the proposed model, the VF becomes thinner when the shear thinning viscosity of the gel viscosity is effective, whereas the VF becomes wider when the gel behaves as an elastic or solid material and, thus, acts to reduce the permeability of the porous media. The aforementioned viscoelastic properties are based on actual viscosity measurements of the gel bulk itself. Combining the experimental results and theoretical considerations demonstrates that the opposite effects, dependent on the gel strength, are driven by the fact that the rheological properties, which are mainly responsible for the flow dynamics, change depending on the gel strength.

In reacting flows, it is well recognized that the flow changes more significantly as the change in the fluid properties, induced by the reaction, increases. Specifically, the flow changes monotonically in response to the change in the physical properties induced by the reaction. However, this paper clearly demonstrates that the effect on the flow reverses depending on the degree of change in the physical properties of the fluid due to the reaction in the reacting flow involving the gel production. This is because the viscoelastic properties of the gel differently affect flow dynamics depending on the gel strength (here, the shear thinning viscosity property is effective when the gel strength

is medium, whereas the elastic property is effective when the gel strength is high). In Fig. 6 in Ref. [48], the patterns of VF with production of viscoelastic material as a function of the reactant concentration under a fixed flow rate were reported. The patterns seem to nonmonotonically change with the reactant concentration. We note that the authors of Ref. [48] did not take the results shown in Fig. 6 as such. The results could be similar to the present main findings, i.e., the nonmonotonic effect of the gel strength on the VF pattern under a fixed flow rate. However, in Ref. [48], the systematic rheological measurement of the gel as a function of the reactant concentrations was not performed. This paper will help to elucidate origin of the nonmonotonic effects observed in Ref. [48].

Control of flow dynamics utilizing change in fluid properties induced by chemical reaction is called chemical control of flow. The chemical control of flow is based on an idea such that the flow monotonically changes more significantly as the change in the fluid properties due to the reaction is larger. However, this paper shows that the above idea is not always correct in chemical control of flow with production of viscoelastic material. Therefore, this paper can lead the reacting flow research to a different stage and open avenues for flow control using chemical reactions. In fact, it was reported that in the application of chemical control of flow with viscoelastic material to enhanced oil recovery in three-dimensional porous media, VF dynamics become more stable by the reaction, which results in a significant increase in the oil recovery [76,77]. Also, it was reported that thinned VF of gastric acid in the mucus layer in gastric epithelium, which is pointed out to be driven by gel produced by the acid and mucus, is responsible for a mechanism by which gastric acid is transported inside the stomach without damaging the gastric mucosa [78]. The present paper will contribute to elucidate such reversal of effects of production of viscoelastic materials on flow dynamics observed in the example of chemical control of flow with viscoelastic material or the application of reacting flow with production of viscoelastic material.

ACKNOWLEDGMENTS

This paper was supported by KAKENHI Grants from the Japan Society for the Promotion of Science (JSPS) (Grants No. 22686020, No. 25630049, and No. 16K06068). We are grateful to Professor Y. Tada and Professor S. Iwata of Nagoya Institute of Technology, M. Takano of TA Instruments Japan, Inc., Professor M. Mishra of the Indian Institute of Technology Ropar, and T. Ujiie who was a former student of the Nagoya Institute of Technology for a fruitful discussion.

-
- [1] R. J. Kee, M. E. Coltrin, P. Glarborg, and H. Zhu, *Chemically Reacting Flow: Theory, Modeling, and Simulation*, 2nd ed. (Wiley, Hoboken, NJ, 2017).
 - [2] C. Almarcha, P. M. J. Trevelyan, P. Grosfils, and A. De Wit, Chemically Driven Hydrodynamic Instabilities, *Phys. Rev. Lett.* **104**, 044501 (2010).
 - [3] J. T. H. Andres and S. S. S. Cardoso, Onset of convection in a porous medium in the presence of chemical reaction, *Phys. Rev. E* **83**, 046312 (2011).
 - [4] D. A. Bratsun and A. De Wit, Buoyancy-driven pattern formation in reactive immiscible two-layer systems, *Chem. Eng. Sci.* **66**, 5723 (2011).
 - [5] C. Almarcha, P. M. J. Trevelyan, P. Grosfils, and A. De Wit, Thermal effects on the diffusive layer convection instability of an exothermic acid-base reaction front, *Phys. Rev. E* **88**, 033009 (2013).
 - [6] V. Loodts, L. Rongy, and A. De Wit, Chemical control of dissolution-driven convection in partially miscible systems: Theoretical classification, *Phys. Chem. Chem. Phys.* **17**, 29814 (2015).
 - [7] J. J. Hidalgo, M. Dentz, Y. Cabeza, and J. Carrera, Dissolution patterns and mixing dynamics in unstable reactive flow, *Geophys. Res. Lett.* **42**, 6357 (2015).
 - [8] M. Chan Kim, Effect of the irreversible $A + B \rightarrow C$ reaction on the onset and the growth of the buoyancy-driven instability in a porous medium: Asymptotic, linear, and nonlinear stability analyses, *Phys. Rev. Fluids* **4**, 073901 (2019).

- [9] J. Martin, N. Rakotomalala, D. Salin, and M. Böckmann, Buoyancy-driven instability of an autocatalytic reaction front in a Hele-Shaw cell, *Phys. Rev. E* **65**, 051605 (2002).
- [10] A. De Wit, Fingering of Chemical Fronts in Porous Media, *Phys. Rev. Lett.* **87**, 054502 (2001).
- [11] J. Yang, A. D’Onofrio, S. Kalliadasis, and A. De Wit, Rayleigh-taylor instability of reaction-diffusion acidity fronts, *J. Chem. Phys.* **117**, 9395 (2002).
- [12] A. De Wit, Miscible density fingering of chemical fronts in porous media: Nonlinear simulations, *Phys. Fluids* **16**, 163 (2004).
- [13] L. Lemaigre, M. A. Budroni, L. A. Riolfo, P. Grosfils, and A. De Wit, Asymmetric Rayleigh-Taylor and double-diffusive fingers in reactive systems, *Phys. Fluids* **25**, 014103 (2013).
- [14] P. M. J. Trevelyan, C. Almarcha, and A. De Wit, Buoyancy-driven instabilities around miscible $A + B \rightarrow C$ reaction fronts: A general classification, *Phys. Rev. E* **91**, 023001 (2015).
- [15] V. Loodts, P. M. J. Trevelyan, L. Rongy, and A. De Wit, Density profiles around $A + B \rightarrow C$ reaction-diffusion fronts in partially miscible systems: A general classification, *Phys. Rev. E* **94**, 043115 (2016).
- [16] V. Loodts, C. Thomas, L. Rongy, and A. De Wit, Control of Convective Dissolution by Chemical Reactions: General Classification and Application to CO₂ Dissolution in Reactive Aqueous Solutions, *Phys. Rev. Lett.* **113**, 114501 (2014).
- [17] M. A. Budroni, L. A. Riolfo, L. Lemaigre, F. Rossi, M. Rustici, and A. De Wit, Chemical control of hydrodynamic instabilities in partially miscible two-layer systems, *J. Phys. Chem. Lett.* **5**, 875 (2014).
- [18] C. Almarcha, Y. R’Honi, Y. De Decker, P. M. J. Trevelyan, K. Eckert, and A. De Wit, Convective mixing induced by acid-base reactions, *J. Phys. Chem. B* **115**, 9739 (2011).
- [19] C. Almarcha, P. M. J. Trevelyan, L. A. Riolfo, A. Zalts, C. El Hasi, A. D’Onofrio, and A. De Wit, Active role of a color indicator in buoyancy-driven instabilities of chemical fronts, *J. Phys. Chem. Lett.* **1**, 752 (2010).
- [20] S. Kuster, L. A. Riolfo, A. Zalts, C. El Hasi, C. Almarcha, P. M. J. Trevelyan, A. De Wit, and A. D’Onofrio, Differential diffusion effects on buoyancy-driven instabilities of acid-base fronts: The case of a color indicator, *Phys. Chem. Chem. Phys.* **13**, 17295 (2011).
- [21] Y. Nagatsu, K. Matsuda, Y. Kato, and Y. Tada, Experimental study on miscible viscous fingering involving viscosity changes induced by variations in chemical species concentrations due to chemical reactions, *J. Fluid Mech.* **571**, 475 (2007).
- [22] Y. Nagatsu, Y. Kondo, Y. Kato, and Y. Tada, Effects of moderate damköhler number on miscible viscous fingering involving viscosity decrease due to a chemical reaction, *J. Fluid Mech.* **625**, 97 (2009).
- [23] Y. Nagatsu and A. De Wit, Viscous fingering of a miscible reactive $A + B \rightarrow C$ interface for an infinitely fast chemical reaction: Nonlinear simulations, *Phys. Fluids* **23**, 043103 (2011).
- [24] V. Sharma, S. Pramanik, C. Y. Chen, and M. Mishra, A numerical study on reaction-induced radial fingering instability, *J. Fluid Mech.* **862**, 624 (2019).
- [25] D. M. Escala, A. De Wit, J. Carballido-Landeira, and A. P. Munuzuri, Viscous fingering induced by a pH-sensitive clock reaction, *Langmuir* **35**, 4182 (2019).
- [26] S. Sin, T. Suekane, Y. Nagatsu, and A. Patmonojai, Three-dimensional visualization of viscous fingering for non-newtonian fluids with chemical reactions that change viscosity, *Phys. Rev. Fluids* **4**, 054502 (2019).
- [27] P. Shukla and A. De Wit, Influence of the pécelet number on reactive viscous fingering, *Phys. Rev. Fluids* **5**, 014004 (2020).
- [28] M. C. Kim, S. Pramanik, V. Sharma, and M. Mishra, Unstable miscible displacements in radial flow with chemical reactions, *J. Fluid Mech.* **917**, A25 (2021).
- [29] Y. Nagatsu, C. Iguchi, K. Matsuda, Y. Kato, and Y. Tada, Miscible viscous fingering involving viscosity changes of the displacing fluid by chemical reactions, *Phys. Fluids* **22**, 024101 (2010).
- [30] Y. Nagatsu, Y. Kondo, Y. Kato, and Y. Tada, Miscible viscous fingering involving viscosity increase by a chemical reaction with moderate damköhler number, *Phys. Fluids* **23**, 014109 (2011).
- [31] L. A. Riolfo, Y. Nagatsu, S. Iwata, R. Maes, P. M. J. Trevelyan, and A. De Wit, Experimental evidence of reaction-driven miscible viscous fingering, *Phys. Rev. E* **85**, 015304(R) (2012).
- [32] S. Stewart, D. Marin, M. Tullier, J. Pojman, E. Meiburg, and P. Bunton, Stabilization of miscible viscous fingering by a step growth polymerization reaction, *Exp. Fluids* **59**, 114 (2018).

- [33] A. De Wit and G. M. Homsy, Viscous fingering in reaction-diffusion systems, *J. Chem. Phys.* **110**, 8663 (1999).
- [34] T. Gérard and A. De Wit, Miscible viscous fingering induced by a simple $A + B \rightarrow C$ chemical reaction, *Phys. Rev. E* **79**, 016308 (2009).
- [35] S. H. Hejazi and J. Azaiez, Non-linear interactions of dynamic reactive interfaces in porous media, *Chem. Eng. Sci.* **65**, 938 (2010).
- [36] S. H. Hejazi, P. M. J. Trevelyan, J. Azaiez, and A. De Wit, Viscous fingering of a miscible reactive $A + B \rightarrow C$ interface: A linear stability analysis, *J. Fluid Mech.* **652**, 501 (2010).
- [37] J. Fernandez and G. M. Homsy, Viscous fingering with chemical reaction: Effect of *in-situ* production of surfactants, *J. Fluid Mech.* **480**, 267 (2003).
- [38] R. Tiani and L. Rongy, Influence of marangoni flows on the dynamics of isothermal $A + B \rightarrow C$ reaction fronts, *J. Chem. Phys.* **145**, 124701 (2016).
- [39] R. Tsuzuki, T. Ban, M. Fujimura, and Y. Nagatsu, Dual role of surfactant-producing reaction in immiscible viscous fingering evolution, *Phys. Fluids* **31**, 022102 (2019).
- [40] L. A. Riolfo, J. Carballido-Landeira, C. O. Bounds, J. A. Pojman, S. Kalliadasis, and A. De Wit, Experimental reaction-driven liquid film fingering instability, *Chem. Phys. Lett.* **534**, 13 (2012).
- [41] R. Tsuzuki, Q. Li, Y. Nagatsu, and C.-Y. Chen, Numerical study of immiscible viscous fingering in chemically reactive hele-shaw flows: Production of surfactants, *Phys. Rev. Fluids* **4**, 104003 (2019).
- [42] T. Podgorski, M. C. Sostarecz, S. Zorman, and A. Belmonte, Fingering instabilities of a reactive micellar interface, *Phys. Rev. E* **76**, 016202 (2007).
- [43] T. Burghlelea, K. Wielage-Burchard, I. Frigaard, M. D. Martinez, and J. Feng, A novel low inertia shear flow instability triggered by a chemical reaction, *Phys. Fluids* **19**, 083102 (2007).
- [44] T. I. Burghlelea and I. A. Frigaard, Unstable parallel flows triggered by a fast chemical reaction, *J. Non-Newtonian Fluid Mech.* **166**, 500 (2011).
- [45] M. Yamaguchi, R. Hagiwara, T. Yokomori, and T. Ueda, Experimental study on flow characteristics with gel reaction in a non-element mixer, *J. Chem. Eng. Jpn.* **50**, 485 (2017).
- [46] Y. Nagatsu, A. Hayashi, M. Ban, Y. Kato, and Y. Tada, Spiral pattern in a radial displacement involving a reaction-producing gel, *Phys. Rev. E* **78**, 026307 (2008).
- [47] Z. Niroobakhsh and A. Belmonte, Dynamics of a reactive micellar oil-water interface in a flowing liquid column, *J. Non-Newtonian Fluid Mech.* **261**, 111 (2018).
- [48] Z. Niroobakhsh, M. Litman, and A. Belmonte, Flow instabilities due to the interfacial formation of surfactant-fatty acid material in a hele-shaw cell, *Phys. Rev. E* **96**, 053102 (2017).
- [49] M. Yamaguchi, T. Yokomori, and T. Ueda, Quantitative prediction of fluid flow patterns with gel reaction in a circular flow pipe, *J. Chem. Eng. Jpn.* **52**, 593 (2019).
- [50] A. De Wit, Chemo-hydrodynamic patterns and instabilities, *Annu. Rev. Fluid Mech.* **52**, 531 (2020).
- [51] P. G. Saffman and G. Taylor, The penetration of a fluid into a porous medium or hele-shaw cell containing a more viscous liquid, *Proc. R. Soc. London, Ser. A* **245**, 312 (1958).
- [52] G. M. Homsy, Viscous fingering in porous media, *Annu. Rev. Fluid Mech.* **19**, 271 (1987).
- [53] J. Nittmann, G. Daccord, and H. E. Stanley, Fractal growth of viscous fingers: Quantitative characterization of a fluid instability phenomenon, *Nature (London)* **314**, 141 (1985).
- [54] H. Van Damme, F. Obrecht, P. Levitz, L. Gatineau, and C. Laroche, Fractal viscous fingering in clay slurries, *Nature (London)* **320**, 731 (1986).
- [55] E. Lemaire, P. Levitz, G. Daccord, and H. Van Damme, From Viscous Fingering to Viscoelastic Fracturing in Colloidal Fluids, *Phys. Rev. Lett.* **67**, 2009 (1991).
- [56] H. Zhao and J. V. Maher, Associating-polymer effects in a Hele-Shaw experiment, *Phys. Rev. E* **47**, 4278 (1993).
- [57] A. Lindner, D. Bonn, and J. Meunier, Viscous fingering in a shear-thinning fluid, *Phys. Fluids* **12**, 256 (2000).
- [58] A. Lindner, D. Bonn, E. C. Poiré, M. Ben Amar, and J. Meunier, Viscous fingering in non-newtonian fluids, *J. Fluid Mech.* **469**, 237 (2002).
- [59] D. H. Vlad and J. V. Maher, Tip-splitting instabilities in the channel saffman-taylor flow of constant viscosity elastic fluids, *Phys. Rev. E* **61**, 5439 (2000).

- [60] A. Lindner, P. Coussot, and D. Bonn, Viscous Fingering in a Yield Stress Fluid, *Phys. Rev. Lett.* **85**, 314 (2000).
- [61] D. Bonn and J. Meunier, Viscoelastic Free-Boundary Problems: Non-Newtonian Viscosity vs Normal Stress Effects, *Phys. Rev. Lett.* **79**, 2662 (1997).
- [62] S. Malhotra and M. M. Sharma, Impact of fluid elasticity on miscible viscous fingering, *Chem. Eng. Sci.* **117**, 125 (2014).
- [63] G. D. Carvalho, J. A. Miranda, and H. Gadêlha, Interfacial elastic fingering in Hele-Shaw cells: A weakly nonlinear study, *Phys. Rev. E* **88**, 053006 (2013).
- [64] J. V. Fontana, H. Gadêlha, and J. A. Miranda, Development of tip-splitting and side-branching patterns in elastic fingering, *Phys. Rev. E* **93**, 033126 (2016).
- [65] A. He, J. Lowengrub, and A. Belmonte, Modeling an elastic fingering instability in a reactive Hele-Shaw flow, *SIAM J. Appl. Math.* **72**, 842 (2012).
- [66] M. Zhao, A. Belmonte, S. Li, X. Li, and J. Lowengrub, Nonlinear simulations of elastic fingering in a Hele-Shaw cell, *J. Comput. Appl. Math.* **307**, 394 (2016).
- [67] G. D. Carvalho, R. Brandão, and J. A. Miranda, Elastic fingering in two-dimensional stokes flow, *Phys. Rev. Fluids* **5**, 104005 (2020).
- [68] K. C. Tam and C. Tiu, Role of ionic species and valency on the steady shear behavior of partially hydrolyzed polyacrylamide solutions, *Colloid Polym. Sci.* **268**, 911 (1990).
- [69] T. Ueki, J. Iijima, S. Tagawa, and Y. Nagatsu, Unpredictable dynamics of polymeric reacting flow by comparison between pre- and post-reaction fluid properties: Hydrodynamics involving molecular diagnosis via ATR-FTIR spectroscopy, *J. Phys. Chem. B* **123**, 4587 (2019).
- [70] S. Vandebriel, A. Franck, G. G. Fuller, P. Moldenaers, and J. Vermant, A double wall-ring geometry for interfacial shear rheometry, *Rheol. Acta* **49**, 131 (2010).
- [71] T. G. Mezger, *The Rheology Handbook*, 4th ed. (Vincentz Network, 2014), Vol. 38.
- [72] M. Trojer, M. L. Szulczewski, and R. Juanes, Stabilizing Fluid-Fluid Displacements in Porous Media Through Wettability Alteration, *Phys. Rev. Appl.* **3**, 054008 (2015).
- [73] J. D. Chen, Radial viscous fingering patterns in Hele-Shaw cells, *Exp. Fluids* **5**, 363 (1987).
- [74] J. D. Chen, Growth of Radial Viscous Fingers in a Hele-Shaw Cell, *J. Fluid Mech.* **201**, 223 (1989).
- [75] See Supplemental Material at <http://link.aps.org/supplemental/10.1103/PhysRevFluids.7.023201> for a derivation of Eq. (15).
- [76] Y. Nagatsu, K. Abe, K. Konmoto, and K. Omori, Chemical flooding for enhanced heavy oil recovery via chemical-reaction-producing viscoelastic material, *Energy Fuels* **34**, 10655 (2020).
- [77] M. A. Mahardika, Y. She, F. Shori, A. Patmonoaji, S. Matsushita, T. Suekane, and Y. Nagatsu, Enhanced heavy oil recovery by calcium hydroxide flooding with the production of viscoelastic materials: Study with 3-D x-ray tomography and 2-D glass micromodels, *Energy Fuels* **35**, 11210 (2021).
- [78] K. R. Bhaskar, P. Garik, B. S. Turner, J. D. Bradley, R. Bansil, H. E. Stanley, and J. T. LaMont, Viscous fingering of HCl through gastric mucin, *Nature (London)* **360**, 458 (1992).